Available online at BCREC website: https://bcrec.id

Bulletin of Chemical Reaction Engineering & Catalysis, 16 (3) 2021, 481-490

Research Article

Preparation of $NiFe_2O_4$ Nanoparticles by Solution Combustion Method as Photocatalyst of Congo red

Poedji Loekitowati Hariani[1,2,*], Muhammad Said[1,2], Addy Rachmat[1], Fahma Riyanti[1], Handayani Citra Pratiwi[1], Widya Twiny Rizki[3]

[1]Department of Chemistry, Faculty of Mathematics and Natural Sciences, Universitas Sriwijaya, Jalan Palembang-Prabumulih, Indralaya, Indonesia.
[2]Research Centre of Advanced Material and Nanocomposite, Faculty of Mathematics and Natural Sciences, Universitas Sriwijaya, Jalan Palembang-Prabumulih, Indralaya, Indonesia.
[3]Magister Program of Chemistry, Faculty of Mathematics and Natural Sciences, Universitas Sriwijaya, Jalan Padang Selasa, Palembang, Indonesia.

Received: 18th April 2021; Revised: 21st May 2021; Accepted: 22nd May 2021
Available online: 28th May 2021; Published regularly: September 2021

Abstract

$NiFe_2O_4$ nanoparticles had been successfully synthesized by solution combustion method using urea fuel (organic precursor). The synthesized $NiFe_2O_4$ were characterized by X-ray diffraction (XRD), Scanning electron microscopy-Electron Dispersive X-ray Spectroscopy (SEM-EDs), Transmission Electron Microscopy (TEM), Fourier Transform Infra-Red (FTIR), Vibrating Sample Magnetometer (VSM), UV-Vis Diffuse Reflectance Spectroscopy (UV-Vis DRS), and Point of Zero Charge (pHpzc). $NiFe_2O_4$ nanoparticles irradiated with visible light were employed to degrade Congo red dye with the following variable: solution pH (3–8), H_2O_2 concentration (0.5–3 mM), and Congo red concentration (100–600 mg/L). XRD analysis results showed that the $NiFe_2O_4$ nanoparticles had a cubic spinel structure. The particle sizes are in the range of 10–40 nm. The magnetic properties of $NiFe_2O_4$ nanoparticles determined using VSM showed a magnetization saturation value of 47.32 emu/g. UV-Vis DRS analysis indicated that $NiFe_2O_4$ nanoparticles had an optical band gap of 1.97 eV. The success of synthesis was also proven by the EDS analysis results, which showed that the synthesized $NiFe_2O_4$ nanoparticles composed of Ni, Fe, and O elements. The removal efficiency of Congo red dye was 96.80% at the following optimum conditions: solution pH of 5.0, H_2O_2 concentration of 2 mM, Congo red dye concentration of 100 mg/L, and contact time of 60 min. The study of the photodegradation kinetics follows a pseudo-first order reaction with a rate constant value of 0.0853 min^{-1}.

Keywords: $NiFe_2O_4$ nanoparticles; photocatalytic degradation; Congo red dye

How to Cite: P.L. Hariani, M. Said, A. Rachmat, F. Riyanti, H.C. Pratiwi, W.T. Rizki (2021). Preparation of $NiFe_2O_4$ Nanoparticles by Solution Combustion Method as Photocatalyst of Congo red. *Bulletin of Chemical Reaction Engineering & Catalysis*, 16(3), 481-490 (doi:10.9767/bcrec.16.3.10848.481-490)

Permalink/DOI: https://doi.org/10.9767/bcrec.16.3.10848.481-490

1. Introduction

The utilization of synthetic dyes in industries such as textiles, plastics, rubber, cosmetics, and papers generates liquid waste that contains dyes. This waste is harmful to humans, animals, aquatic plants and can be carcinogenic [1,2]. Approximately one million tons of dyestuffs have been synthesized and traded worldwide [3,4]. One of the dyes often used in industry is Congo red. Congo red is an anionic dye that has azo and sulfonate groups. Congo red dyes have been widely used in the textile, tannery, dying, paper, rubber, and plastic industries [1].

* Corresponding Author.
Email: puji_lukitowati@mipa.unsri.ac.id (P.L. Hariani);
Telp: +62-81532730025

Conventional physical, biological, and chemical waste treatment methods are costly, inefficient, and produce secondary pollutants [5]. This problem can be overcome through advanced oxidation processes (AOPs). Photo Fenton reaction is a method of AOPs that often used because it produces oxidative species such as hydroxyl radicals (•OH). This method is based on utilizing semiconducting materials, oxidants, and light sources to degrade the dye.

Spinel ferrite nanomaterials have attracted attention due to their applications in various fields, such as magnetic refrigeration, remarkable electrical, magnetic resonance imaging, catalysis, and magnetic adsorbents [6–8]. Ferrite compounds have the general formula, MFe_2O_4, where iron(III) oxide (Fe_2O_3) is the main component, and M is a divalent metal ion, such as: Ni, Cu, Fe, Zn, Co, and Mg [9]. Photocatalytic degradation is one of the noted usages of ferrite compounds to degrade pollutants in water or wastewater. Photocatalytic degradation using ferrite compounds effectively reduces pollutant toxicity because the pollutants are degraded into smaller and harmless molecules such as H_2O and CO_2 [7]. The ferrite compound is a catalyst that has a stable structure, excellent magnetic properties, and low bandgap energy [10,11]. The separation of ferrite compounds from solutions can be completed without filtration by utilizing external magnets, making them efficient and promising in industrial applications [12].

The mechanism of photocatalyst degradation generally involves the formation of hydroxyl radicals and the formation of superoxide anions from oxygen. When a photocatalyst compound absorbs light with a specific wavelength, the photocatalyst obtains energy. This energy is used for the excitation of electrons from the valence band (VB) to the conduction band (CB). A hole is produced in the VB (h^+), and an electron is produced in the CB (e^+). The resulting hole breaks down water molecules into a hydroxyl radical, which reacts with organic molecules to break down organic compounds [13].

The combination of several oxidation systems causes an increase in the degradation's effectiveness [14]. One such system is H_2O_2. H_2O_2 is harmless to the environment because it is easily broken down into water and oxygen [7]. The degradation method using H_2O_2, known as photo-Fenton oxidation, has been proven to be effective in degrading the dye. However, this method has the drawback of losing the catalyst. Several studies show that the combination of photocatalytic degradation and H_2O_2 provide good degradation performance, as shown by the degradation of methylene blue dyes using Fe_3O_4 compounds [15], degradation of rhodamine B dyes using $CoFe_2O_4$ [7], and degradation of methylene blue dyes using Fe_3O_4/AC/TiO_2 [16].

$NiFe_2O_4$ nanoparticles can be synthesized using sol-gel, coprecipitation, solid-state reaction, chemical reaction, hydrothermal, solvothermal, and solution combustion. The solution combustion method is particularly suitable for synthesizing ferrite nanoparticles due to its simple procedure, rapidity, and low-temperature requirement. The resulting product has high homogeneity and purity [7,17]. Moreover, this method has a high success rate [18]. Several organic compounds, such as: glycine, urea, citric acid, alanine, sucrose, dextrose, and EDTA, can be used as fuel [17,19]. Urea was chosen as the fuel in this study, because it is cheap, safe, and non-toxic [19].

In this study, $NiFe_2O_4$ nanoparticles were synthesized through the solution combustion method using urea as fuel. The resulting $NiFe_2O_4$ nanoparticles were characterized utilizing XRD, SEM-EDS, TEM, FTIR, VSM, UV-Vis DRS, and pHpzc. The $NiFe_2O_4$ nanoparticles were used for photodegradation of Congo red dye in the presence of visible light irradiation. H_2O_2 was added to increase the amount of hydroxyl group that degrades the dye.

2. Materials and Methods

2.1 Materials

All chemicals used, $Ni(NO_3)_2.6H_2O$, $Fe(NO_3)_3.9H_2O$, urea, NaOH, HCl, Congo red dye, and H_2O_2 30%, were obtained from Merck, Germany.

2.2 Synthesis of $NiFe_2O_4$ Nanoparticles

$NiFe_2O_4$ nanoparticles were synthesized through the solution combustion method [7,19]. A total of 6.0 g of urea was dissolved in 50 mL of distilled water. Subsequently, 4.36 g of $Ni(NO_3)_2.6H_2O$ and 12.19 g of $Fe(NO_3)_3.9H_2O$ were added. The mixture was stirred to form a gel then heated at 80 °C for 12 hours in the oven. The solid formed was calcined at 500 °C for three hours at a heating rate of 5 °C/min. The synthesis reaction of $NiFe_2O_4$ nanoparticles is as follows [17]:

$$3Ni(NO_3)_2.6H_2O + 6Fe(NO_3)3.9H_2O + 20(NH_2)_2CO \rightarrow 3NiFe_2O_4 + 112H_2O + 20CO_2 + 32N_2 \quad (1)$$

2.3 Characterization of $NiFe_2O_4$ Nanoparticles

The crystal structure of the $NiFe_2O_4$ nanoparticles was determined using X-ray diffractometer (XRD Rigaku Miniflex-600), in the range of 2θ = 10–90°. Crystal size was determined using the Scherrer equation [20], as follows:

$$D = \frac{k\lambda}{\beta \cos\theta} \quad (2)$$

where D is the average $NiFe_2O_4$ crystal size, λ is the X-ray wavelength (0.15418 nm), k is the Scherrer constant (0.9), β is the full width at half maximum (FWHM), and θ is the Bragg diffraction angle.

The morphology and element composition of the $NiFe_2O_4$ nanoparticles were analyzed using SEM-EDS (JSM 6510) and TEM JEOL JEM 1400. The magnetic properties of the $NiFe_2O_4$ nanoparticles were determined utilizing VSM (Lakeshore 74004). Optical absorption spectra analysis was performed employing UV-Vis DRS (Pharmaspec UV-1700).

The following procedure was employed to determine the pHpzc of $NiFe_2O_4$ nanoparticles. Nine tubes containing 50 mL of 0.01 M NaCl solution were pH adjusted (2–10) using 0.1 M HCl or NaOH. The solution was added with 0.1 g of $NiFe_2O_4$ nanoparticles. The mixture was stirred using a magnetic stirrer for two hours and then left for 24 hours. The final pH of the solution was measured using a pH meter. pHpzc was determined based on a graph plot of the initial pH of the solution and ΔpH.

2.4 Photocatalytic Activity of $NiFe_2O_4$ Nanoparticles

The photocatalytic activity of $NiFe_2O_4$ nanoparticles was evaluated based on their ability to degrade Congo red. A total of 0.05 g of $NiFe_2O_4$ was added to 50 mL of 200 mg/L Congo red dye solution. The experiment was carried out in a closed reactor at room temperature. Each sample was irradiated with visible light (10–60 min) with a fixed distance of 15 cm using a 60-watt Philips compact lamp. After the photocatalytic degradation process, $NiFe_2O_4$ nanoparticles were separated from the solution using an external magnet. The concentration of the remaining Congo red dye was determined using a UV-Vis spectrophotometer (Genesys 10S). The effect of H_2O_2 and the concentration of Congo red dye were investigated by varying the amount of H_2O_2 (0.5-3.0 mM) and the concentration of Congo red (100-600 mg/L). The following formula was used to calculate the effectiveness of removal.

$$Removal\ efficiency = \frac{C_0 - C_t}{C_0} \quad (3)$$

where C_0 dan C_t are initial and final concentrations of Congo red dye (mg/L), respectively.

3. Results and Discussion

3.1 Characterization of $NiFe_2O_4$ Nanoparticles

In this study, $NiFe_2O_4$ nanoparticles were synthesized using urea as fuel by solution combustion method. XRD was utilized to investigate the structure of $NiFe_2O_4$ nanoparticles. Figure 1 shows the XRD peaks of the synthesized $NiFe_2O_4$ nanoparticles. The structure of the $NiFe_2O_4$ was cubic spinel, according to JCPDS $NiFe_2O_4$ (Card No. 10-0325), which was observed at 2θ =10–90°. Sharp peaks appeared at 2θ = 35.12° (311), whereas other peaks appeared at 2θ = 30.35° (220), 38.06° (222), 44.06° (400), 53.96° (422), 57.28° (511), and 63.80° (440). The $NiFe_2O_4$ crystal size average was

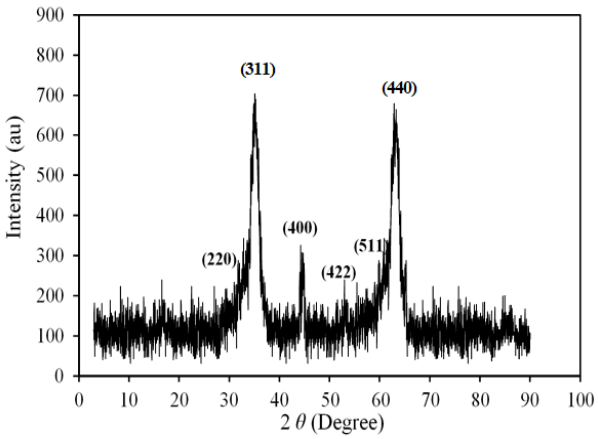

Figure 1. XRD pattern of the $NiFe_2O_4$ nanoparticles.

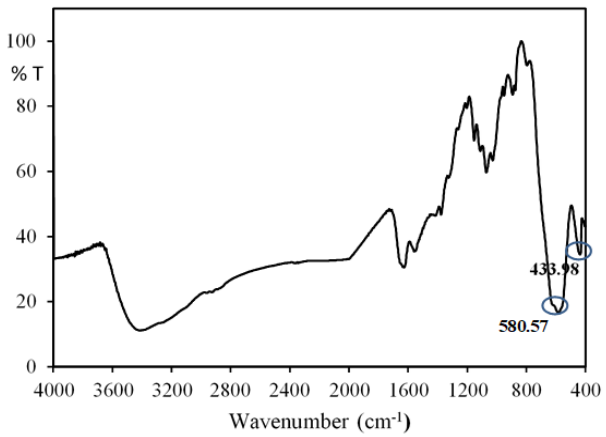

Figure 2. FTIR Spectra of the $NiFe_2O_4$ nanoparticles.

calculated using the Scherrer equation was 8.6 nm. This crystal size was smaller than the $NiFe_2O_4$ synthesized via the sol-gel method (25–45 nm) [8] and the coprecipitation method (18 nm) [21].

The characterization results of $NiFe_2O_4$ nanoparticles using FTIR at a wavenumber of 400–4000 cm^{-1} is shown in Figure 2. In general, FTIR spectra are distinguished in two regions, namely wave numbers 100–1000 and 1000–4000 cm^{-1} [22]. The metal oxide functional groups are observed at wavenumbers below 1000 cm^{-1}. The spinel structure was confirmed from two peaks at wavenumbers of 580–620 and 420–435 cm^{-1} [9]. In this study, a strong peak was detected at 580.57 cm^{-1} which indicated the stretching vibration of nickel and oxygen bonds (Ni–O), whereas the wave number at 433.98 cm^{-1} pointed to the stretching vibration of iron and oxygen (Fe–O) bonds. The wide spectrum observed at the wave number 3200–3500 cm^{-1} indicates the OH group's stretching vibration. This functional group originated from the absorbed water.

The magnetic properties of $NiFe_2O_4$ nanoparticles were determined using VSM at room temperature. The saturation magnetization (M_s) of $NiFe_2O_4$ nanoparticles was calculated from the hysteresis curve. Figure 3 shows the hysteresis curve of $NiFe_2O_4$ nanoparticles. This curve indicates that $NiFe_2O_4$ nanoparticles are superparamagnetic. The magnetization saturation value obtained was 47.32 emu/g. The typical magnetization saturation is related to small particle size [23]. Magnetic properties are influenced by crystallite size. The smaller crystallite size indicates poor crystallinity. The increase in crystallite size is increasing saturation magnetization [24]. The magnetization saturation value of $NiFe_2O_4$ calculated using the Neel sublattice theory for the inverse cubic spinel of $NiFe_2O_4$ nanoparticles is 50 emu/g, whereas the value for bulk $NiFe_2O_4$ is 56 emu/g [25]. The saturation magnetization in this study obtained was greater than the $NiFe_2O_4$ nanoparticles synthesized using the same method with glycine, sucrose, and glycerol as fuels, namely 20, 8, and 8 emu/g [17].

The optical absorption properties of $NiFe_2O_4$ nanoparticles studied using UV-Vis DRS are shown in Figure 4. UV-Vis DRS was used to demonstrate the photo-absorption ability of the synthesized sample [26]. The analysis showed that the $NiFe_2O_4$ nanoparticles could absorb energy in visible light region. Strong absorption appeared at a wavelength of 423 nm. The direct optical band gap value of the $NiFe_2O_4$ nanoparticles, which was calculated using the Kulbeka Munk equation based on the Taut plot $[F®hv]^2$ versus hv was 1.97 eV, which was smaller than the value found in the literature 2.19 eV [27]. The band gap of $NiFe_2O_4$

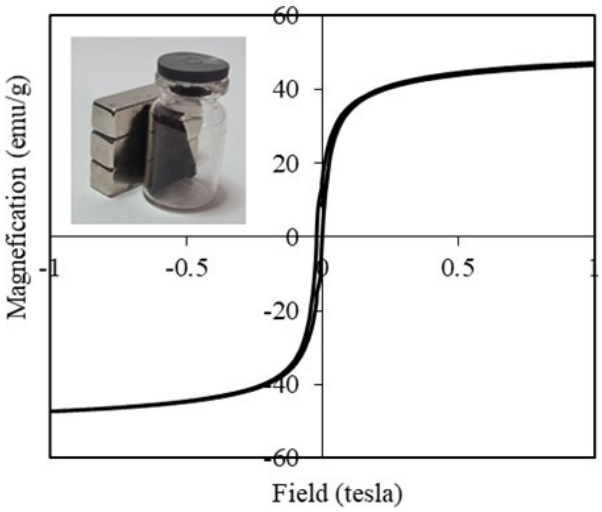

Figure 3. Magnetic properties of $NiFe_2O_4$ nanoparticles.

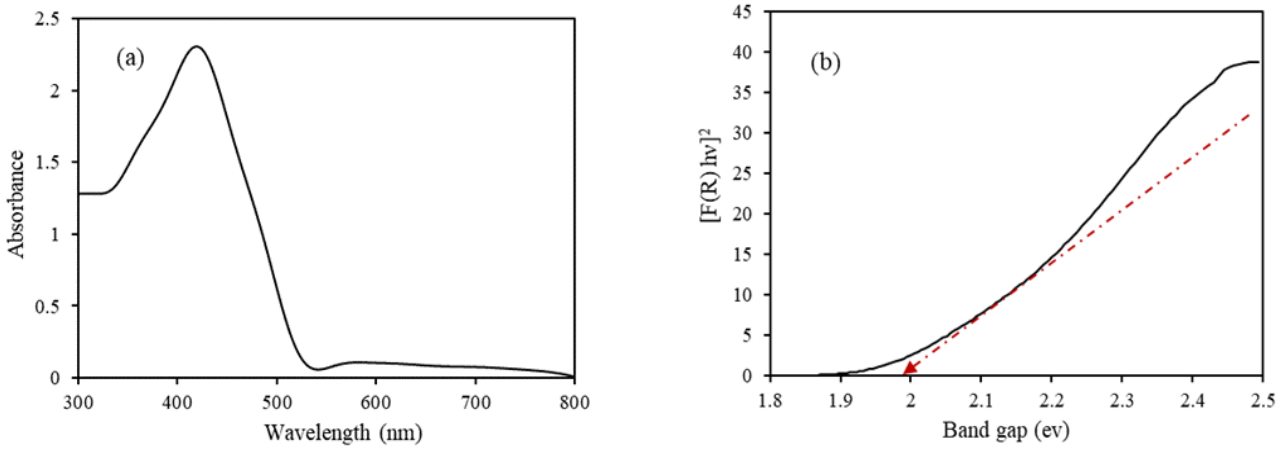

Figure 4. Spectra of (a) UV-Vis DRS and (b) band gap energies of the $NiFe_2O_4$ nanoparticles.

nanoparticles synthesized was greater than by the coprecipitation method, namely 1.64 eV [28] and 1.87 eV [29]. The band gap energy of ferrite compounds is 2.0 eV, which is effective for absorbing visible light [30].

Figure 5 shows the SEM and TEM image of the $NiFe_2O_4$ nanoparticles. The structure and shape of particles vary greatly depending on the synthesis method used [6]. The morphology of the $NiFe_2O_4$ nanoparticles indicated that the particles underwent agglomeration. Particles with a small size tend to agglomerate. The particle sizes of $NiFe_2O_4$ nanoparticles in the range of 10–40 nm. Based on the EDS data, the element composition of the $NiFe_2O_4$ nanoparticles was 14.70% Ni, 38.20% Fe, and 47.10% O. This composition confirmes that the successful synthesis of the $NiFe_2O_4$ nanoparticles.

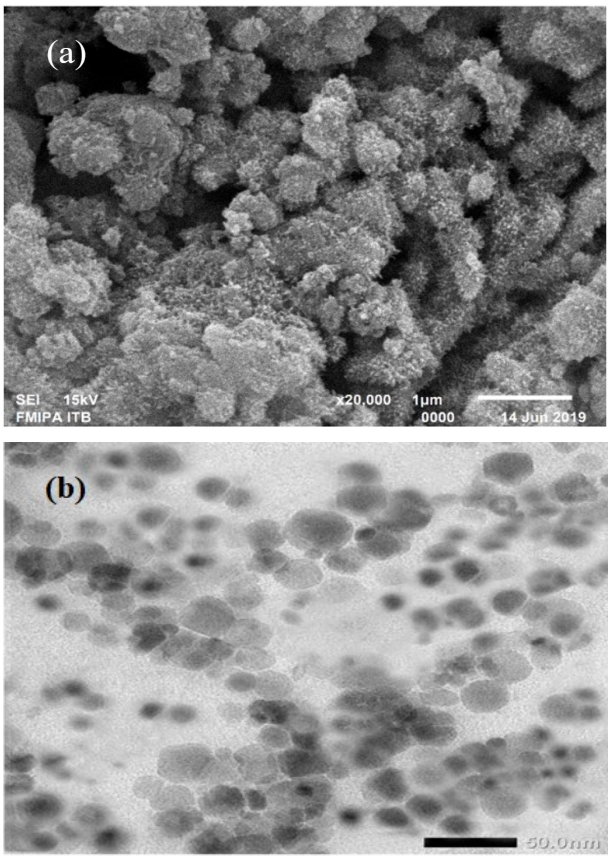

Figure 5. (a) SEM image, (b) TEM image, and (c) EDS spectra of the $NiFe_2O_4$ nanoparticles.

3.2 Photocatalytic Degradation of Congo red Dye

The photocatalytic degradation of Congo red dye using $NiFe_2O_4$ nanoparticles was carried out at a solution pH of 3–8. The Congo red dye's natural pH (5.6) affected the electrostatic interaction between $NiFe_2O_4$ nanoparticles and the dye. Figure 6 shows the pHpzc of $NiFe_2O_4$ nanoparticles, which was 6.8. This result was almost identical to that in Mouinpour's study [31], whereas $NiFe_2O_4$ nanoparticles synthesized using the coprecipitation method had a pHpzc of 6.7. At pH conditions below pHpzc, $NiFe_2O_4$ nanoparticles are positively charged, and Congo red is an anionic dye. This electrostatic attraction will increase the effectiveness of the degradation.

The effect of pH on degradation was investigated in the pH range of 3–8 with an initial dye concentration of 200 mg/L and a time variation of 10–60 min. Figure 6 shows that at pH 3 to 5, the photocatalytic degradation's effec-

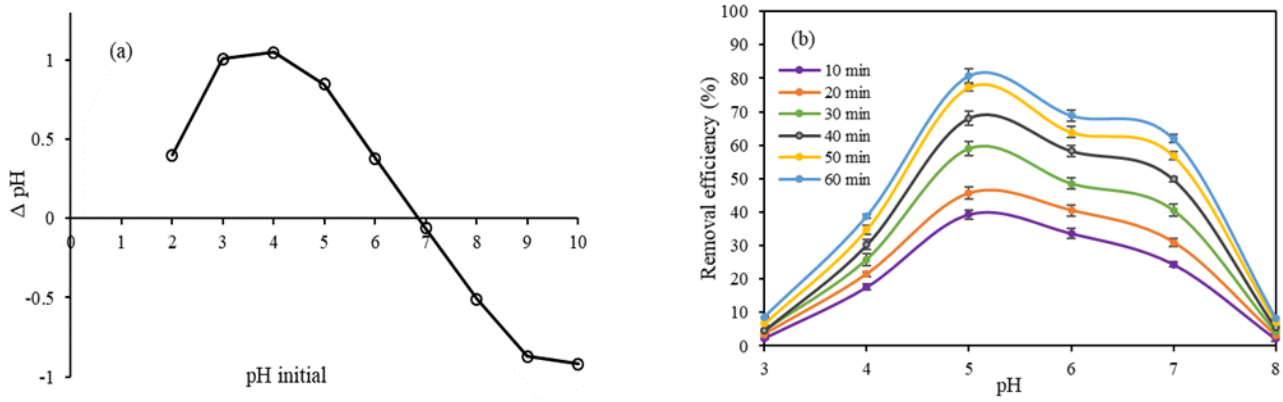

Figure 6. (a) pHpzc and (b) effect of pH on the degradation of Congo red dye.

tiveness increased and then decreased. The peak effectiveness of removal was achieved at a solution pH of 5. The decrease in the effectiveness at higher pH condition can be explained due to an increase of OH^- in solution causing $Fe(OH)_3$ deposition [32]. The process of dye degradation using $NiFe_2O_4$ is as follows [8]:

$$NiFe_2O_4 + h\nu \rightarrow NiFe_2O_4 (e^- + h^+) \quad (4)$$
$$NiFe_2O_4 (e^-) + O_2 \rightarrow NiFe_2O_4 + \cdot O_2^- \quad (5)$$
$$NiFe_2O_4 (h^+) + OH^- \rightarrow NiFe_2O_4 + \cdot OH \quad (6)$$
$$\cdot O_2^- + H_2O \rightarrow HO_2\cdot + OH^- \quad (7)$$
$$\cdot OH + \text{Congo red} \rightarrow \text{degradation product} \quad (8)$$
$$\cdot O_2^- + \text{Congo red} \rightarrow \text{degradation product} \quad (9)$$
$$HO_2\cdot + \text{Congo red} \rightarrow \text{degradation product} \quad (10)$$

Figure 7(a) demonstrates the effect of H_2O_2 on the effectivity of Congo red removal. The addition of 0.5-3.0 mM H_2O_2 increased the effectiveness of degradation. The effectiveness was relatively constant after 2.0 mM H_2O_2 was added. The photodegradation of methylene blue using $MnFe_2O_4$ nanoparticles showed an identical trend, where the addition of H_2O_2 increased the effectiveness of removal to a specific concentration. Subsequently, the effectiveness remained constant [12]. The most remarkable effectiveness was observed with 2.0 mM H_2O_2 addition. The addition of H_2O_2 increases the amount of $HO_2\cdot$ and $\cdot OH$ radicals, thereby increasing the degradation process. $NiFe_2O_4$ nanoparticles contain Fe^{3+} ions that react with H_2O_2 according to the following reaction [33,34]:

$$Fe^{3+} + H_2O_2 \rightarrow Fe^{2+} + H^+ + HO_2\cdot \quad (11)$$
$$Fe^{3+} + HO_2\cdot \rightarrow Fe^{2+} + O_2 + H^+ \quad (12)$$
$$Fe^{2+} + H_2O_2 + H^+ \rightarrow Fe^{3+} + \cdot OH + H_2O \quad (13)$$

The effectiveness of removal at the addition of 2.5 to 3.0 mM H_2O_2 was relatively constant. $\cdot OH$ radical can react in parallel with excess H_2O_2 to produce $HO_2\cdot$ and H_2O. Afterwards, some $\cdot OH$ radicals react with $HO_2\cdot$ to produce H_2O_2 and O_2. The subsequence reaction reduces the effectiveness of hydroxyl radicals in degrade the dye [35]. The reactions that occur are as follows:

$$\cdot OH + \text{Dye} \rightarrow \text{degradation product} \quad (14)$$
$$\cdot OH + H_2O_2 \rightarrow HO_2\cdot + H_2O \quad (15)$$
$$\cdot OH + HO_2\cdot \rightarrow H_2O_2 + \tfrac{1}{2}O_2 \quad (16)$$

The effect of the initial concentration of the Congo red dye was investigated by varying the dye's concentration in the range of 100–600 mg/L. The experiment was carried out with 25 mL of the Congo red solution and 0.05 g of $NiFe_2O_4$ nanoparticles at a pH of 5.0 for 10–60 min. Figure 7(b) shows that the optimum photocatalytic degradation achieved at 100 mg/L with a contact time of 60 min, where the removal efficiency was 96.80%. The removal efficiency was reversely proportional to the concentration of the Congo red dye. This phenomenon occurs because the active part of the catalyst has been filled with dye molecules, whereas the amount of catalyst was constant [36].

3.3 Effect of Visible Light Irradiation

$NiFe_2O_4$ nanoparticles, with the help of visible light irradiation, instigate electrons to move to CB, leaving electron holes in VB [37]. Subsequently, a reaction with water occurs, producing hydroxyl radicals that degrade the dye into intermediate compounds with shorter carbon chains and simpler compounds [8,12].

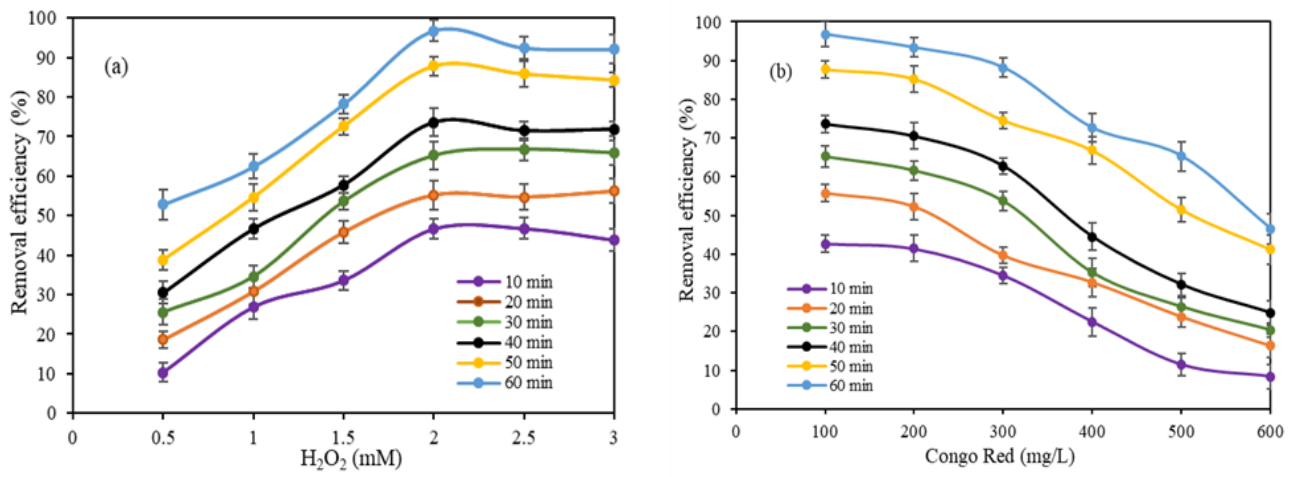

Figure 7. Effect of (a) H_2O_2 concentration and (b) Congo red dye concentration on photocatalytic degradation.

H_2O_2 plays a role in multiplying the number of hydroxyl radicals, thus accelerating the degradation process. The effectiveness of Congo red dye degradation with and without radiation showed a significant difference, as shown in Figure 8. The duration of irradiation also affects the degradation effectiveness [35].

3.4 Kinetic Photocatalytic Degradation

The photocatalytic activity of $NiFe_2O_4$ nanoparticles to the degradation of Congo red dye under visible light irradiation is presented in Figure 9. The kinetic equation is expressed as follows:

$$\ln\left(\frac{C_0}{C_t}\right) = kt \quad (17)$$

where C_0 and C_t are initial concentrations and concentrations at any given time of the Congo red dye, and k is the velocity constant. The activity of $NiFe_2O_4$ nanoparticles as a photocatalyst increased with increasing reaction time. The photocatalytic activity following a pseudo-first-order reaction. The $[\ln(C_0/C_t)]$ versus t curve showed a linear relationship with a correlation coefficient (R^2) of 0.9906 and a rate constant value (k) of 0.0853 min^{-1}. The k value of a linear regression shows the ability of the catalyst to degrade the dye [36]. The half-life time value obtained was $t_{1/2} = 0.693/k = 8.12$ min. Another study showed that the degradation of dye by $NiFe_2O_4$ nanoparticles followed pseudo-first order show in Table 1.

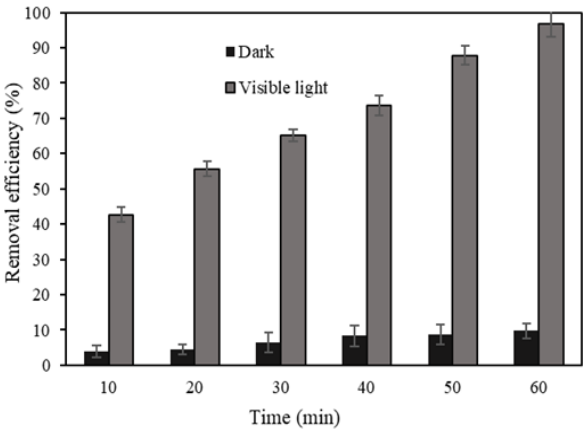

Figure 8. Removal efficiency of Congo red dye with and without visible light irradiation (100 mg/L of Congo red dye concentration, 0.05 g $NiFe_2O_4$, and 2 mM H_2O_2 on solution pH of 5.0).

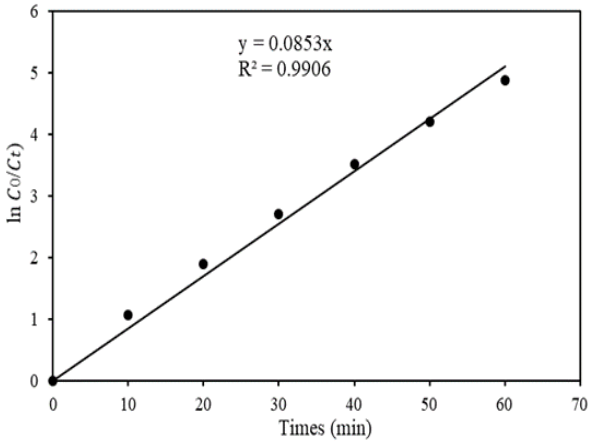

Figure 9. Kinetic photocatalytic degradation of Congo red dye.

Table 1. The pseudo-first order kinetics degradation of several dyes by $NiFe_2O_4$ nanoparticles.

Dye	Experiment	Irradiation source	k [min^{-1}]	Ref.
Methylene blue	[MB] = 10 mg/L, catalyst dosage = 10 mg	Visible	0.003	[38]
Methylene blue	[MB] = 10^{-5} M, catalyst dosage = 0.01 g	Visible	0.002	[39]
Irrgalite violet	[IV] = 200 mg/L, [Oxalic acid] = 2 mM, pH = 3, catalyst dosage = 0.15 g	Sunlight	-0.00223	[32]
Malachite green	[MG] = 10^{-5} M, catalyst dosage = 1 g, pH =5.8–5.9	Visible light	0.00343	[40]
Methylene blue	[MB] = 10^{-5} M, catalyst dosage = 0.01 g	Visible light	0.002	
Methylene blue	[MB] = 30 mg/L, catalyst dosage = 20 mg	Microwave electrodeless discharge lamp	0.08137	[41]
Congo red	[CR] = 100 mg/L, pH = 5, [H_2O_2] = 2 mM	Visible light	0.0853	Present study

4. Conclusions

In this study, $NiFe_2O_4$ nanoparticles were successfully synthesized through the solution combustion method using urea as fuel. The $NiFe_2O_4$ nanoparticles had a particle size in the range 10–40 nm and showing a saturation magnetization value of 47.32 emu/g. The combination of $NiFe_2O_4$ nanoparticles, H_2O_2, and visible light irradiation was adequate for the photocatalytic degradation of Congo red dyes. The optimum condition for photocatalytic degradation was accomplished using the following variables: solution pH of 5, H_2O_2 concentration of 2 mM, 100 mg/L Congo red dye concentration, and contact time of 60 min. The removal effectiveness of Congo red dye achieved was 96.80%. Therefore, $NiFe_2O_4$ nanoparticles had excellent catalytic activity.

Acknowledgment

The authors would like to express gratitude to Sriwijaya University for providing research funding in the form of a *Hibah Profesi* scheme with contract number 0174.05/UN9/SB3.LPPM.PT/2020.

References

[1] Farias, R.S., Buargue, H.L.B., Cruz, M.B., Cardoso, L.M.F., Gondim, T.A., Paulo, V.R. (2018). Adsorption of Congo Red Dye from Aqueous Solution onto Amino-Funtionalized Silica Gel. *Engenharia Sanitaria e Ambiental*, 23, 1053–2060. DOI: 10.1590/S1413-41522018172982

[2] Guo, X., Wang, K., Qin J. (2017). Heterogeneous Photo-Fenton Processes Using Graphite Carbon Coating Hollow $CuFe_2O_4$ Spheres for the Degradation of Methylene Blue. *Applied Surface Science,* 420, 792–801. DOI: 10.1016/j.apsusc.2017.05.178

[3] Zu, Y., Zhao, Y., Xu., K., Tong, Y., Zhao, F. (2016). Preparation and Comparison of Catalytic Performance for Nano $MgFe_2O_4$, GO-loaded $MgFe_2O_4$ and GO-coated $MgFe_2O_4$ nanocomposites. *Ceramics Internasional*, 42, 18844–18850. DOI: 10.1016/j.ceramint.2016.09.030

[4] Rashad, M.M. (2007). Magnetic Properties of Nanocrystalline Magnesium Ferrite by Co-precipitation assisted with Ultrasound Irradiation. *Journal of Material Science*, 42, 5248–5255. DOI 10.1007/s10853-006-0389-9.

[5] Khan, A., Valicsek, Z., Horvath, O. (2020). Synthesis, Characterization and Application of Iron (II) Doped Copper Ferrites ($Cu^{II}(x)Fe^{II}(1-x)Fe^{III}_2O_4$) as Novel Heterogeneous Photo-Fenton Catalysts. *Nanomaterials*, 10, 921–938. Doi: 10.3390/nano10050921.

[6] Kombaiah, K., Vijaya, J.J., Kennedy, L.J., Kaviyarasu, K. (2019). Catalytic Studies of $NiFe_2O_4$ Nanoparticles Prepared by Conventional and Microwave Combustion Method. *Materials Chemistry and Physics*, 221, 11–28. DOI: 10.1016/j.matchemphys.2018.09.012.

[7] Nguyen, L.T.T., Nguyen, L.T.H., Manh. N.C., Quoc, D.N., Quang, H.N., Nguyen, H.T.T., Nguyen, D.C., Bach, L.G. (2019). A Facile Synthesis, Characterization, and Photocatalytic Activity of Magnesium Ferrite Nanoparticles via The Solution Combustion Method. *Journal of Chemistry*, 2019, 1–9. DOI: 10.1155/2019/3428681.

[8] Talebi, R. (2017). Preparation of Nickel Ferrite Nanoparticles via A New Route and Study of Their Photocatalytic Properties. *Journal of Materials Science*, 28, 4058–4063. DOI: 10.1007/s10854-016-6020-1.

[9] Hirthna, H., Sendhilnathan, S., Rajan, P.I., Adinaveen, T. (2018). Synthesis and Characterization of $NiFe_2O_4$ Nanoparticles for the Enhancement of Direct Sunlight Photocatalytic Degradation of Methyl Orange. *Journal of Superconductivity and Novel Magnetism*, 31, 1–9. DOI: 10.1007/s10948-018-4601-3.

[10] Wang, Y., Zhao, H., Li, M., Fab, J., Zhao, G. (2014). Magnetic Ordered Mesoporous Copper Ferrite as a Heterogeneous Fenton Catalyst for the Degradations of Imidacloprid. *Applied Catalysis B Environmental*, 147, 534–545. DOI: 10.1016/j.apcatb.2013.09.017.

[11] Zhang, X., Geng, Z., Jian, J., He, Y., Lv, Z., Liu, X., Yuan, H. (2020). Potassium Ferrite as Heterogeneous Photo-Fenton Catalyst for Highly Efficient Dye Degradation. *Catalysis*, 10, 1–9. DOI: 10.3390/catal10030293.

[12] Desai, H.B., Hathiya, L.J., Joshi, H.H., Tanna, A.R. (2020). Synthesis and Characterization of Photocatalytic $MnFe_2O_4$ Nanoparticles. *Materials Today*, 21, 1905–1010. DOI: 10.1016/j.matpr.2020.01.248.

[13] Sonu, Dutta, V., Sharma, S, Raizada, P., Bandegharaei, A.H., Gupta, V.K., Singh, P. (2019). Review on Augmentation in Photocatalytic Activity of $CoFe_2O_4$ via Heterojunction Formation for Photocatalysis of Organic Pollutants in Water. *Journal of Saudi Chemical Society*, 23, 1119–1136. DOI: 10.1016/j.jscs.2019.07.003.

[14] Kuriechen, S.K., Murugesan, S., Raj, S.P. (2013). Mineralization of Azo Dye Using Combined Photo-Fenton and Photocatalytic Processes under Visible Light. *Journal of Catalysis*, 2013, 1–6. DOI: 10.1155/2013/104019.

[15] Yan, P., Gao, L., Li, W. (2014). Microwave-enhanced Fenton-like System, Fe_3O_4/H_2O_2 for Rhodamine B Wastewater Degradation. *Applied Mechanics and Materials*, 448, 834–837. DOI: 10.4028/www.scientific.net/AMM.448-453.834.

[16] Moosavi, S., Li, R.Y.M., Lai, C.W., Yusof, Y., Gan, S., Akbarzadeh, O., Chowhury, Z.Z., Yue, X.G., Johan, M.R. (2020). Synthesized Fe_3O_4/AC/TiO_2 Nano-Catalyst: Degradation and Reusability Studies. *Nanomaterials*, 10, 1–15. DOI: 10.3390/nano10122360.

[17] Lazarova, T., Georgieva, M., Tzankov, D., Voykova, D., Aleksandrov, L., Zheleva, Z.C., Kovacheva, D. (2017). Influence of Type of Fuel for the Solution Combustion Synthesis on the Structure, Morphology and Magnetic Properties of Nanosized $NiFe_2O_4$. *Journal of Alloys and Compounds*, 700, 272–283. DOI: 10.1016/j.jallcom.2017.01.055.

[18] Egizbek, K., Kozlovskiy, A.L., Ludzik, K., Zdorovets, M.V., Korolkov, L.V., Marciniak, B., Jazdzewska, M., Chudoba, D., Nazarova, A., Kontek, R. (2020). Stability and Cytotoxicity Study of $NiFe_2O_4$ Nanocomposites Synthesized by Coprecipitation and Subsequent Thermal Annealing. *Ceramics Internasional*, 46, 16548–16555. DOI: 10.1016/j.ceramint.2020.03.222.

[19] Karakas, Z.K., Boncukcuoglu, R., Karakas, I.H., (2016). The effects of Fuel in Synthesis of $NiFe_2O_4$ Nanoparticles by Microwave Assisted Combustion Method. In *Proceedings of the Internasional Physics Conference at the Anatolian Peak. Journal of Physics: Conferences Series,* 707, 1–11. DOI: 10.1088/1742-6596/707/1/012046.

[20] Sagadevan, S., Chawdhury, Z.Z., Rafique, R.E. (2016). Preparation and Characterization of Nickel Ferrite Nanoparticles via Coprecipitation Method. *Material Research*, 21, 1–5. DOI: 10.1590/1980-5373-mr-2016-0533.

[21] Lin, C.C., Ho, J.M. (2014). Structural analysis and Catalytic Activity of Fe3O4 Nanoparticles Prepared by a Facile Coprecipitation Method in a Rotating Packed Bed. *Ceramics Internasional*, 40, 10275–10282. DOI: 10.1016/j.ceramint.2014.02.119.

[22] Balaji, S., Selvan, R.K., Berchmans, L.J., Angappan, S., Subramanian, K., Augustin, C.O. (2005). Combustion Synthesis and Characterization of Sn^{4+} Substituted Nanocrystalline $NiFe_2O_4$. *Materials Science and Engineering B*, 119, 119–124. DOI: 10.1016/j.mseb.2005.01.021.

[23] Zhang, D., Tong, Z., Xu, G., Li, S., Ma, J. (2009). Template Fabrication of $NiFe_2O_4$ Nanorods: Characterization, Magnetic, and Electrochemical Properties. *Solid State Sciences*, 11, 113–117. DOI: 10.1016/j.solidstatesciences.2008.05.001.

[24] Das, H., Inukai, A., Debnath, N., Kawaguchi, T., Sakamoto, N., Hoque, S.M., Aono, H., Shinazaki, K., Suzuki, H., Wakiya, N. (2018). Influence of Crystallite on the Magnetic and heat Generation Properties of $La_{0.77}Sr_{0.23}MnO_3$ Nanoparticles for Hyperthermia Applications. *Journal of Physics and Chemistry of Solids*, 112, 179–184. DOI: 10.1016/j.jpcs.2017.09.030.

[25] Tan, J., Zhang, W., Xia, A. (2013). Facile Synthesis of Inverse Spinel $NiFe_2O_4$ Nanocrystals and Their Superparamagnetic Properties. *Materials Research*, 16, 237–241. DOI: 10.1590/S1516-143920120050000157.

[26] El Desouky, F.G., Saadeldin, M.M., Mahdy, M.A., El Zawawi, I.K. (2021). Tuning the Structure, Morphological Variations, Optical and Magnetic Properties of $SnO_2/NiFe_2O_4$ Nanocomposites for Promising Applications. *Vacuum*, 185, 1–12. DOI: 10.1016/j.vacuum.2020.110003.

[27] Xu, S., Shangguan, W., Yuan, J., Chen, M., Shi, J. (2007). Preparation and Photocatalytic Properties of Magnetically Separable Nitrogen-Doped TiO_2 Supported on Nickel Ferrite. *Applied Catalysis B. Environmental*, 71, 177–184. DOI: 10.1016/j.apcatb.2006.09.004.

[28] Rahmayeni, Zulhadjri, Jamarun, N., Emriadi, Arief, S. (2016). Synthesis of ZnO-$NiFe_2O_4$ Magnetic Nanocomposites by Simple Solvothermal Method for Photocatalytic Dye Degradation under Solar Light. *Oriental Journal of Chemistry*, 32, 1411–1419. DOI: 10.13005/ojc/320315.

[29] Quinonez, J.L.O., Pal, U., Villanueva, M.S. (2018). Structural, Magnetic, and Catalytic Evaluation of Spinel Co, Ni, and Co-Ni Ferrite Nanoparticles Fabricated by Low-Temperature Solution Combustion Process. *ACS Omega*, 3, 14986–15001. DOI: 10.1021/acsomega.8b02229.

[30] Casbeer, E., Sharma, V.K., Li, X.Z. (2012). Synthesis and Photocatalytic Activity of Ferrites under Visible Light: A review. *Separation and Purification Technology*, 87, 1–14. DOI: 10.1016/j.seppur.2011.11.034.

[31] Moeinpour, F., Kamyab, S., Akhgar, M.R. (2017). $NiFe_2O_4$ Magnetic Nanoparticles as an Adsorbent for Cadmium Removal from Aqueous Solution. *Journal of Water Chemistry and Technology*, 39, 281–288. DOI: 10.3103/S1063455X17050058.

[32] Vijay, S., Balakrishnan, R.M., Rene, E.R., Priyanka, U. (2019). Photocatalytic Degradation of Irgalite Violet Dye using Nickel Ferrite Nanoparticles. *Journal of Water Supply: Research and Technology-Aqua*, 68, 666–674. DOI: 10.2166/aqua.2019.039.

[33] Zhou, L., Lei, J., Wang, L., Liu, Y., Zhang, J. (2017). Highly Efficient Photo-Fenton Degradation of Methyl Orange Facilitated by Slow Light Effect and Hierarchical Porous Structure of Fe_2O_3-SiO_2 Photonic Crystal. *Applied Catalysis B Environmental*, 237, 1160–1167. DOI: 10.1016/j.apcatb.2017.08.039.

[34] Rezai, P., Baniyaghoob, S., Sadr, M.H. (2019). Fe_3O_4@SiO_2@AgO Nanocomposite: Synthesis, Characterization, and Investigation of its Photocatalytic Application, *Journal of Electronic Materials*, 48, 3285–3296. DOI: 10.1007/s11664-019-07091-z.

[35] Flores, A., Nesprias, K., Vitale, P., Tasca, J., Lavat, A., Eyler, N., Canizo, A. (2014). Heterogeneous Photocatalytic Discoloration/Degradation of Rhodamine B with H_2O_2 and Spinel Copper Ferrite Magnetic Nanoparticles. *Australian Journal of Chemistry*, 67, 609–614. DOI: 10.1071/CH13435.

[36] Ameta, N., Sharma, J., Chanderia, K. (2012). Degradation of Crystal Violet using Copper Modified Iron Oxide as Heterogeneous Photo-Fenton Reagent. *Journal of Iranian Chemical Research*, 5, 241–253.

[37] Sakwises, L., Pisitsak, P., Manuspiya, H., Ummartyotin, S. (2017). Effect of Mn-substituted SnO_2 Particle Toward Photocatalytic Degradation of Methylene Blue Dye. *Results in Physics*, 7, 1751–1759. DOI: 10.1016/j.rinp.2017.05.009.

[38] Patil, S.S., Tamboli, M.S., Deonikar, V.G., Umarji, G.G., Ambekar, J.D., Kulkami, M.V., Kolekar, S.S., Kale, B.B., Patil, D.R. (2015). Magnetically Separable Ag_3PO_4/$NiFe_2O_4$ Composites with Enhanced Photocatalytic Activity, *Dalton Transactions*, 44, 20426–20434. DOI: 10.1039/c5dt03173g.

[39] Kahhki, R.M., Khorrampoor, A., Rabbani, M., Ahsani, F. (2017). Visible Light Photocatalytic Degradation of Textile Waste Water by Co Doped NiFe2O4 Nanocomposite. *Journal of Materials Science: Materials in Electronics*, 28, 4095–4101. DOI: 10.1007/s10854-016-6028-6.

[40] Tsvetkov, M.P., Ivanova, I.R., Valcheva, E.P., Zaharieva, J.Ts., Milanova, M.M. (2019). Photocatalytic Activity of $NiFe_2O_4$ and $Zn_{0.5}Ni_{0.5}Fe_2O_4$ Modified by Eu(III) and Tb(III) for Decomposition of Malachite Green. *Open Chemistry*, 17, 1124–1132. DOI: 10.1515/chem-2019-0116.

[41] Wong, Y., Wang, H., Yang, Y., Xin, B. (2021). Magnetic $NiFe_2O_4$ 3D Nanosphere Photocatalyst: Glycerol-Assisted Microwave Solvothermal Synthesis and Photocatalytic Activity under Microwave Electrodeless Discharge Lamp. *Ceramics International*, 47, 14594–14602. DOI: 10.1016/j.ceramint.2021.02.041.